Segmentation of sperm's Acrosome, Nucleus and Mid-piece in microscopic images of stained human semen smear

Ahmad Bijar[1], Mohammad Mikaeili[1], Antonio Peñalver Benavent[2], and Rasoul Khayati[1]
[1]Department of Biomedical Engineering, Shahed University, Tehran, Iran
[2]Center of Operations Research University Institute Miguel Hernández University of Elche, Spain
bijar@shahed.ac.ir, mikaili@shahed.ac.ir, a.penalver@umh.es, khayati@shahed.ac.ir

***Abstract*—The measurement or evaluation and clinical significance of human sperm morphology has always been and still is a controversial aspect of the semen analysis for the determination of a male's fertility potential. The evaluation of sperm size, shape and morphological smear characteristics should be assesed by carefully observing a stained sperm sample under a microscope. In order to avoid subjectivity, numerous studies that incorporate image analysis techniques in the assessment of sperm morphology have been proposed. The primary step of all these methods is segmentation of sperm's parts. In this paper, we have proposed a new method for segmentation of sperm's Acrosome, Nucleus and Mid-piece. Sperm's Acrosome, Nucleus and Mid-piece are segmented through a method based on a Bayesian classifier which utilizes the adaptive mixtures method (AMM) and Markov random field (MRF) model to obtain and upgrade the class conditional probability density function (CCPDF) and the $apriori$ probability of each class. To compare the performance of the proposed approach with those of previous approaches including manual segmentation, the Accuracy, Sensitivity and Specificity were calculated.**

***Index Terms*—Sperm, Segmentation, Bayesian classification, Adaptive Mixture Method, Markov Random Field Model.**

I. Introduction

The measurement or evaluation and clinical significance of human sperm morphology has always been and still is a controversial aspect of the semen analysis for the determination of a male's fertility potential. The evaluation of sperm morphology was and still is regarded as subjective due to the fact that it has to be done by the human eye. Even today most of the modern-day computer-assisted sperm morphology analysis systems still largely depend on human operator skills and are suffering from the same technical problems as manual of sperm morphology evaluation [1]. So, manual procedures are "inexact, subjective, no repeatable, difficult to teach" [2], and computerized techniques are essential tools. The majority of these computer methods have been developed to analyze human sperm morphology and have afterwards been adapted for other species [3]. The development of new methodologies is an ongoing research activity [4], [5]. These researches have enriched the available knowledge on sperm cells [6] and furthermore, digital image analysis had allowed to classify subpopulations [7] or to describe shape abnormalities [5]. Most of these approaches use CASA systems [8], [9] that deploy image processing techniques or propose new description and classification methods [10]–[14]. Some other methods have been developed to analyze human sperm morphology, the primary steps of all these methods is sperm segmentation and discrimination. Sánchez *et al*. [3], [15] and Nowshiravan *et al*. [16] proposed methods based on morphological operators and thresholding to segment sperm's head, because the Acrosome and the Mid-piece have similar characteristics (intensity level, texture) the segmentation with traditional techniques (thresholding, region growing) does not give good results [16], [17]. To tackle this problem, Carrillo *et al*. [18], [19] presented an approach called nth-$fusion$ for segmentation of sperm's Acrosome, Nucleus and Mid-piece in a computer aided tool for the objective analysis of human sperm morphology, commonly known as Automated Sperm Morphology Analyzer (ASMA). After enclosing individual sperms (head and mid-piece) using bounding boxes, they used nth-$fusion$ method which was based on nth-$level$ thresholding of an image followed by intersection with n special masks. In order to obtain the desired segmentation results, a $prior$ objects morphological model, which was based on the information fusion technique in a feature level was used. For each segmented sperm in image, they had to run the algorithm to detect sperm's parts.

In this paper we have proposed a fully automatic method for segmentation of sperm's Acrosome, Nucleus and Mid-piece that requires no training and atlas. At first, an improved hybrid method [20] is used to remove noise from the sperm image (R component of RGB color image). Then, a simple threshold is applied to build a primary mask containing sperm's Acrosome, Nucleus, Mid-piece, and also small objects is seminal plasma. The small objects have been eliminated and to build the final localized mask, the minimum area bounding box of each individual region is computed through the *Rotating Calipers* method [21], [22]. The detection rate and speed have been increased using the bounding boxes. Pixels inside the bounding boxes are considered as samples. Distribution function of the samples is estimated by a mixture of a large number of normal terms through adaptive mixtures method (AMM). Then, the mixture terms are categorized into three classes, as the class conditional probability density functions and the $apriori$ probabilities of the classes. In the next steps, $apriori$

978-1-4577-1473-3/12/$26.00 ©2012 IEEE

probabilities of the classes as well as mean and variance of class conditional probability density function for each class are attained and updated utilizing a Markov random field (MRF) model and AMM, respectively. In the next sections, details of the research procedure including segmentation of sperm's Acrosome, Nucleus and Mid-piece are explained.

II. Materials and Methods

A. Image Acquisition Technique

Sample Images were acquired from modified Papanicolaou stained sperm smears. Fresh Sperm samples were incubated for 30 to 60 minute in 37° Celsius. The Smear was then prepared after complete liquefaction and the slides were dried in the air before staining with modified Papanicolaou method. The images were captured by means of a 560 TV-line CCD camera mounted on the third eyepiece of a trinocular direct microscope (Proway BK5000) with a total magnification of 1000X using Plan Achromatic Infinity objective lenses and a resolution of 576×764 pixels in RGB color space. 10 to 25 Images of different fields were captured from each slide. And totally 100 slides were analyzed (each slide consists of 1 to 5 sperms).

B. Preprocessing

To create a primary mask containing sperm's Acrosome, Nucleus and Mid-piece, the Red component of RGB color image is used. The Red component contains most of the information associated with the darkest color, which domains the head. To remove noise, an improved hybrid method [20] is applied. This method consists of two stages. The first stage consists of a fourth order partial differential equation (PDE) and the second stage is a relaxed median filter, which processes the output of fourth order PDE. This model enjoys the benefit of both nonlinear fourth order PDE and relaxed median filter. By using a relaxed median filter we can preserve more image details than the standard median filter. This method preserves fine details, sharp corners and thin lines and curved structures to large extent. Then, a simple threshold is applied to build a primary mask which contains sperm's Acrosome, Nucleus and Mid-piece, and also small objects is seminal plasma ($< thr$). The threshold value is calculated according to $thr = \mu - \sigma$, in which μ and σ are mean and standard deviation of the noise-removed image, respectively. The small objects have been eliminated and this mask, containing sperm's Acrosome, Nucleus and Mid-piece is used to build the final mask at the next step. To build the final mask, the minimum area bounding box of each individual region is computed through the *Rotating Calipers* method [21], [22]. This method is capable of computing the minimum area enclosing rectangle in linear time. To apply *Rotating Calipers* method, the two dimensional convex hull of all visible points (for each region) is computed using the *monotone chain* algorithm [23]. This algorithm is linear with respect to the number of input points $O(n)$, assuming that input points are sorted by increasing x and increasing y coordinates.

C. Problem Formulation

A finite mixture model $p(\mathbf{x})$ is the weighted sum of $M > 1$ components in $\mathbb{R}^n$ for $n \geqslant 1$:

$$p(\mathbf{x}) = \sum_{m=1}^{M} \pi_m p(\mathbf{x}|m) \quad \forall \mathbf{x} \in \mathbb{R}^n, \tag{1}$$

where $\pi_m \in (0,1)(m = 1, 2, ..., M)$ corresponds to the weight of each component which satisfies $\sum_{m=1}^{M} \pi_m = 1$. For the Gaussian mixtures model, each component density $p(\mathbf{x}|m)$ is a Gaussian probability density given by

$$\begin{aligned} p(\mathbf{x}|\theta_m) \quad = \quad & \frac{1}{(2\pi)^{\frac{n}{2}} det(\sum_m)^{\frac{1}{2}}} \times \\ & exp\left\{-1/2(\mathbf{x}-\mu_m)^T \sum_m^{-1}(\mathbf{x}-\mu_m)\right\} \end{aligned} \tag{2}$$

where T denotes the transpose operation, μ_m is the mean vector and σ_m is the covariance matrix which is assumed positive definite. Here we encapsulate these parameters into a parameter vector, writing the parameters of each component as $\theta_m = (\mu_m, \sum_m)$, to get $\Theta(\pi_1, \pi_2, ..., \pi_M, \theta_1, \theta_2, ..., \theta_M)$. Eq. 1 can be rewritten as

$$p(\mathbf{x}|\Theta) = \sum_{m=1}^{M} \pi_m p(\mathbf{x}|\theta_m) \tag{3}$$

If we knew the component from which $\mathbf{x}$ came, then it would be simple to determine the parameters Θ. Similarly, if we knew the parameters Θ , we could determine the component that would be most likely to have produced $\mathbf{x}$. The difficulty is that we know neither.

D. Estimation of probability density function by AMM

To estimate $p(x|w_j)$ the AMM [24] is used. The AMM utilizes all the data, one by one, to determines the distance of each observation to each component density in the model. In this method, there is a threshold and if the distance to component is more than the threshold, a new component is created. However, if the distance is less than the threshold for all components, the estimated parameters will be updated on the basis of the recursive EM equations. According to this method, an estimation of $p(x|w_j)$ (i.e., $\hat{f}_{AM}(X)$) is computed as below

$$\hat{f}_{AM}(X) = \sum_{i=1}^{N} \hat{p}_i \phi(X; \hat{\mu}_i, \hat{\Sigma}_i) \tag{4}$$

where $\hat{p}_i, \hat{\mu}_i, \hat{\Sigma}_i$ are the estimations of coefficient, mean, and covariance matrix of ith multivariate Gaussian density $\phi(X; \hat{\mu}_i, \hat{\Sigma}_i)$, respectively.

The following features can be mentioned as the advantages of the AMM algorithm in comparison with the EM algorithm [25]:

1) The AMM does not require an initial knowledge for the number of terms.

2) It does not require an initial guess for the term parameters.
3) As the whole data are not used simultaneously for updating the estimation of term parameters, the required calculation is much lower than that of EM especially while we have a massive data set.
4) In contrast to the EM algorithm, the convergence of AMM and also number of iterations do not depend on the tolerance (i.e., a preset threshold for algorithm termination), initial parameters, and the data load.

E. Computation of the a priori *probability by MRF model*

An advantage of MRF models [26] is the use of neighborhood information to improve the $apriori$ probabilities [27] $p(w)$. The intuition behind the MRF model is that most pixels belong to the same class as their neighbors, and it is a powerful tool to describe the class assigning or labeling dependence between adjacent pixels. Suppose a digital image bases on a $M \times N$ lattice, So image describes as $S = \{s = (x, y)|1 \leq x \leq M, 1 \leq y \leq N\}$. Assuming that the unobserved random field $w(x, y)$ is a Markov random field with the probability density function of $w(x, y)$ of a segmented image depending on its finite neighboring region $N(x, y)$, then

$$p(w(x,y)|w(x_i,y_j), \forall (x_i,y_j) \neq (x,y)) \quad = \\ p(w(x,y)|N(x,y)) \tag{5}$$

where $N(x, y)$ is a set of all labeled neighbors. So, the segmentation problem defined as a pixel classification problem using MAP can be estimated using a Gibbs distribution [28], which is easier to estimate. The Gibbs distribution can be expressed as

$$p(w(x,y)|N(x,y)) = \frac{1}{Z} \exp^{-\frac{1}{T}U(w(x,y))} \tag{6}$$

where, $Z = \sum_{w(x,y)} \exp^{-\frac{1}{T}U(x,y)}$ is a normalization constant which guarantees that $p(w(x, y))$ is always smaller or equal to one, and T is a constant which stands for the temperature constant which normally supposes to be one. And the energy function

$$U(w(x,y)) = \sum_{w(x_i,y_j) \in C(x,y)} V(w(x_i,y_j)) \tag{7}$$

where, cliques $C(x, y)$ are subsets of $N(x, y)$ or $w(x, y)$ itself and $V(w(x_i, y_j))$ is an arbitrary function of $w(x, y)$. The equivalence between MRF and Gibbs distribution is expressed by Hammersley-Clifford theorem, which states that $w(x, y)$ is a MRF with neighborhoods $N(x, y)$ if and only if $w(x, y)$ is a Gibbs distribution field with the cliques $C(x, y)$ induced by the neighborhood $N(x, y)$. This theorem provides an easy way to construct the MRF in an explicit manner, i.e., one can explicitly estimate the conditional probability distribution of MRF by choosing specific kinds of cliques $C(x, y)$ and an appropriate energy function $U(w(x, y))$ that is specific for the practical problem.

In our model we used the simple equation for the $U(w)$ energy function proposed by Therrien [29], and utilized by Nett *et al*. [30]. This equation is a linear combination of products of elements in the cliques

$$U(w(x,y)) \quad = \\ w(x,y)(\alpha + \beta_1(w(x-1,y) + w(x+1,y)) \\ + \quad \beta_2(w(x,y-1) + w(x,y+1)) \tag{8}$$

The parameters α, β_1, and β_2 are parameters that allow for adjusting relative weights or contributions of neighborhood interactions. The parameters of MRF model, i.e., α, β_1, and β_2 have been experimentally set to 0.1, 0.01, and 0.01 for the best result. These weightings allow the current classification at index (x, y) to take an importance somewhat greater than the neighborhood classifications, and gives equal weighting to the neighbors of the feature measured at (x, y).

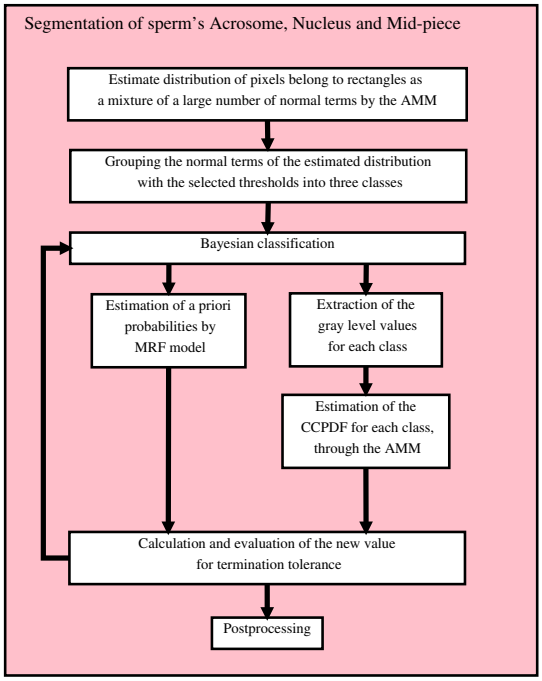

Fig. 1. Block diagram of the proposed approach for fully automatic segmentation of sperm's Acrosome, Nucleus and Mid-piece.

F. Algorithm

Based on the explanations mentioned above, the block diagram of our method for segmentation of sperm's Acrosome, Nucleus and Mid-piece is shown in Fig. 1, and is summarized below

1) Smoothing the R component of RGB color image using a gaussian filter.
2) Selection of pixels inside the boundding boxes as input samples.
3) Estimation of input samples distribution as a mixture of a large number of normal terms by the AMM (i.e., $\hat{p}_{\text{terms}} = \{\hat{p}_1, ..., \hat{p}_N\}$, $\hat{\mu}_{\text{terms}} = \{\hat{\mu}_1, ..., \hat{\mu}_N\}$, and $\hat{\sigma}^2_{\text{terms}} = \{\hat{\sigma}^2_1, ..., \hat{\sigma}^2_N\}$. It is reminded that for univariate case (one feature), the covariance matrix is replaced by the variance of each term.

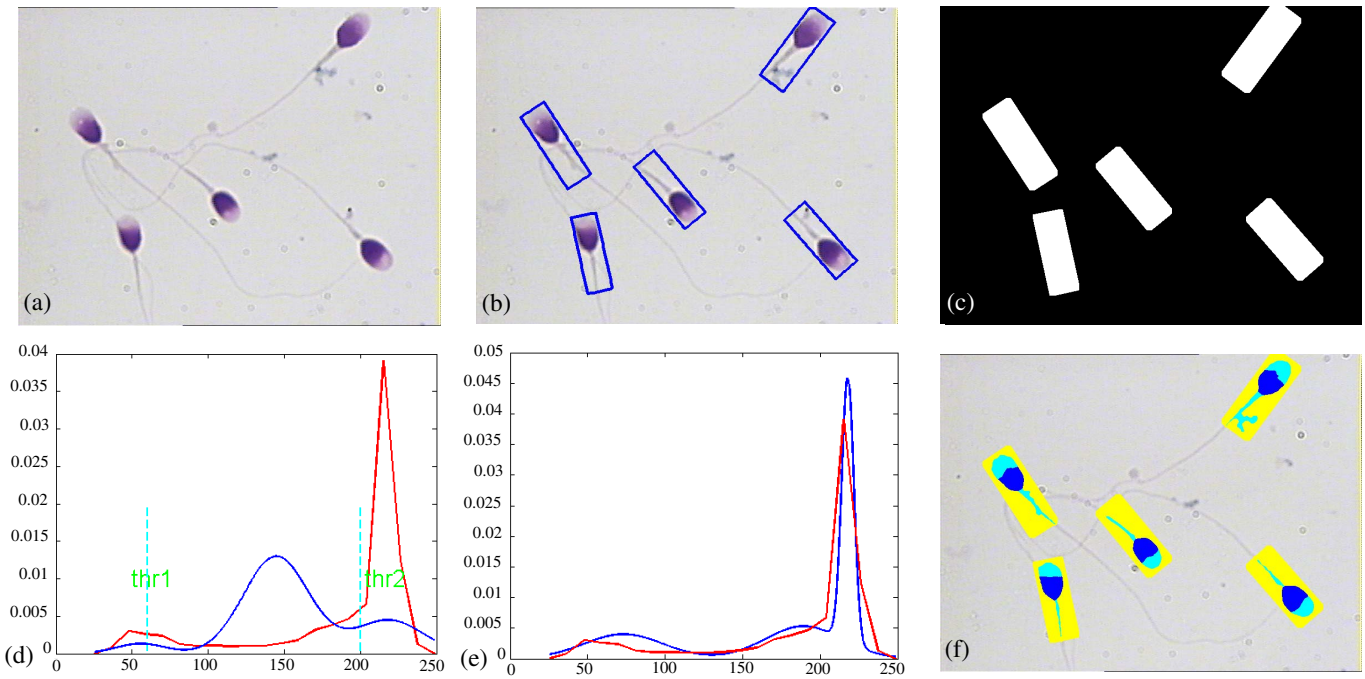

Fig. 2. Result of applying the proposed algorithm to a typical sperm image: (a) Original RGB color image. (b) *Bounding boxes* containing sperm's Acrosome, Nucleus and Mid-piece. (c) Pixels inside the bounding boxes are considered as samples. (d) The resulted distribution by thresholding (blue) overlaid on distribution of the samples (red). (e) Distribution of the samples (red), overlaid on it's final estimation (blue). (f) Result of fully automatic segmentation. (For interpretation of the references to color in this figure, the reader is referred to the web version of this article.)

4) Selection of thresholds for terms grouping. The thresholds value is calculated according to $\text{thr}_1 = \mu_{\text{in}} - 2\sigma_{\text{in}}$ and $\text{thr}_2 = \mu_{\text{in}}$, in which $\mu_{\text{in}}, \sigma_{\text{in}}$ are mean and standard deviation of the input image, respectively.
5) Grouping the normal terms of the estimated distribution with the selected thresholds into three classes as the CCPDFs of classes. Indeed, initial values for parameters (i.e., $\hat{p}_{\text{init}}(w_j)$, $\hat{\mu}_{\text{init}}(w_j)$ and $\hat{\sigma}^2_{\text{init}}(w_j)$) are estimated. The $\hat{\mu}_{\text{init}}$ is calculated according to

$$\hat{\mu}_{\text{init}}(w_j) = \tag{9}$$

$$\begin{cases} \text{mean}\{\mu \in \hat{\mu}_{\text{terms}} | \hat{\mu}_{\text{terms}} < \text{thr1}\} & \text{for } j = 1 \\ \text{mean}\{\mu \in \hat{\mu}_{\text{terms}} | \text{thr1} \leq \hat{\mu}_{\text{terms}} \leq \text{thr2}\} & \text{for } j = 2 \\ \text{mean}\{\mu \in \hat{\mu}_{\text{terms}} | \hat{\mu}_{\text{terms}} < \text{thr3}\} & \text{for } j = 3 \end{cases}$$

in which, j denotes jth class. Also, the variances $(\hat{\sigma}^2_{\text{init}}(w_j))$ and the coefficients $(\hat{p}_{\text{init}}(w_j))$ of these classes are equal to mean of the variances and sum of the coefficients of corresponding terms, respectively.
6) Bayesian classification of the input image (only pixels inside the bounding boxes) using initial values of parameters.
7) Extraction of the gray level values for each class resulted from previous step.
8) Estimation of the CCPDF (i.e., $\hat{\mu}_k(w), \hat{\sigma}^2_k(w)$) for each class, through the AMM.
9) Estimation of *apriori* probabilities (i.e., $\hat{p}_k(w)$) for classes, by MRF model stated in Eqs. 6 to 8.
10) Calculation and evaluation of the new value for termination tolerance. The new value of termination tolerance is calculated from

$$tol = \max \begin{pmatrix} \max(abs(\hat{p}_k(w) - \hat{p}_{k-1}(w)), \\ \max(abs(\hat{\mu}_k(w) - \hat{\mu}_{k-1}(w)), \\ \max(abs(\hat{\sigma}_k(w) - \hat{\sigma}_{k-1}(w)), \end{pmatrix} \tag{10}$$

in which $\hat{p}_k(w)$, $\hat{\mu}_k(w)$, and $\hat{\sigma}_k(w)$ are the row vectors of the *apriori* probabilities, mean, and variance of the tissue classes in kth iteration, respectively.
11) Repetition of steps 6-10 or termination of the computation.
12) Postprocessing: Acrosome and Mid-piece are classified into the same class (i.e., two separated areas as one class). These two areas are grouped into two separated classes (i.e., Acrosome and Mid-piece) using their positions respect to the Nucleus and *bounding box* corners. At first, the distance between each corner of *bounding box* and center of Nucleus is computed. Then, the corner whose value is less than others is considered as *origin*. Acrosome is the region whose distance from *origin* is less than Mid-piece (other region).

III. Results

Figure 2 shows the results of the proposed algorithm, including estimated distribution obtained through the AMM with maximum 25 Gaussian terms overlaid on distribution of the samples (inside the bounding boxes) and selection of the thresholds. Fig. 2(d) shows grouping of the normal

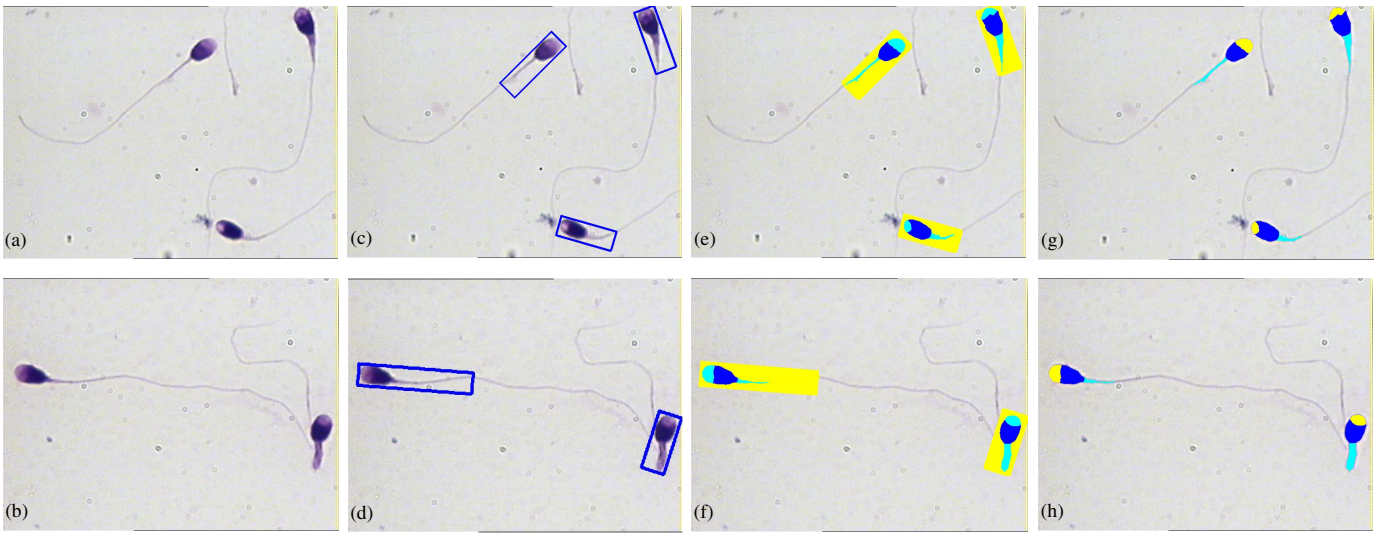

Fig. 3. Result of applying the proposed method to three sperm images : (a) and (b) The original RGB color images. (c) and (d) *Bounding boxes* in the original RGB color images. (e) and (f) Three obtained classes through the proposed method. (g) and (h) Results of fully automatic segmentation. (For interpretation of the references to color in this figure, the reader is referred to the web version of this article.)

terms obtained by AMM into three classes with the selected thresholds, as the distribution functions of the classes. The resulted distribution, overlaid on distribution of the samples with MSE less than 1×10^{-6}, have been shown in Fig. 2(e). In Fig. 3, results of applying the proposed algorithm to other sperm images have been shown. To evaluate the results of the Sperm segmentation based on the proposed method with the entire image database, the following three statistical metrics were employed for comparison: Accuracy (A_c), Sensitivity (S_e) and Specificity (S_p).

$$\begin{aligned} \mathrm{A}_c &= \frac{\mathrm{TN+TP}}{\mathrm{TN+TP+FP+FN}} \\ \mathrm{S}_e &= \frac{\mathrm{TP}}{\mathrm{TP+FN}} \\ \mathrm{S}_p &= \frac{\mathrm{TN}}{\mathrm{TN+FP}} \end{aligned} \tag{11}$$

where, TP stands for true positive, FP for false positive, TN for true negative, and FN for false negative. The evaluation is summarized in Table I. Also the Accuracy of sperm's head, Acrosome, Nucleus and Mid-piece are computed 95.1%, 93.3%, 95.7% and 91.4%, respectively.

TABLE I
EVALUATION RESULTS FOR DETECTION AND EXTRACTION OF INDIVIDUAL SPERMATOZOON

Total Spermatozoa	283
Detected Spermatozoa (TP)	277
Not detected Spermatozoa (FN)	6
Total artifacts	127
True negative or non detected artifacts (TN)	123
Detected artifacts as Spermatozoa (FP)	4
Accuracy (A_c)	96.56%
Sensitivity (S_e)	97.87%
Specificity (S_p)	96.85%

IV. Discussion

In this paper a new approach, for fully automatic segmentation of sperm's Acrosome, Nucleus and Mid-piece in microscopic images of stained human semen smear that requires no training and atlas, is proposed. At first, to increase the detection rate and speed, a localized mask containing sperm's Acrosome, Nucleus and Mid-piece is built through the minimum area bounding boxes. This procedure is done using an improved hybrid method and the *Rotating Calipers* algorithm. Pixels inside the bounding boxes are considered as samples. Distribution function of samples is estimated by a mixture of a large number of normal terms by AMM. Then, the mixture terms are categorized into three classes, as the CCPDFs and the *apriori* probabilities of the classes. In the next steps, *apriori* probabilities of the classes as well as parameters of the classes (i.e., means and variances) are attained and updated, utilizing MRF model and AMM, respectively, and without any need for training samples. Our proposed approach is evaluated via Accuracy, Sensitivity and Specificity in a data set of microscopic images of stained human semen smear. These results were compared with the results, previously, reported by other researcher such as Carrillo *et al*. [18], which used similar methods of evaluation. It is reminded that Carrillo *et al*. [18] used manual segmentation for evaluation of their methods. We, too, used manual segmentation for evaluation. They used similar methods of evaluation. Therefore comparison of our method with this method is reasonable. This comparison is done in Table II. As it is seen in Table II, the proposed method in this paper improves the accuracy of segmentations.

TABLE II
ACCURACY (A_c) VALUES FOR THE PROPOSED METHOD AND CARRILLO *et al*. [18]

Segmentation	Carrillo *et al*. [18]	Proposed method
Head	89.5%	95.1%
Acrosome	88.9%	93.3%
Nucleus	88.9%	95.7%
Mid-Piece	85.0%	91.4%

V. CONCLUSIONS

In this paper a new approach, based on a Bayesian classifier, for automatic segmentation of sperm's Acrosome, Nucleus and Mid-piece in microscopic images of stained human semen smear is proposed. The proposed method utilizes the adaptive mixtures method (AMM) and Markov random field (MRF) model to obtain and upgrade the class conditional probability density function (CCPDF) and the $apriori$ probability of each class (as sperm's parts). The experimental results show the promise of our approach. We are currently exploring new methods for estimation of the morphological characteristics of the sperm.

REFERENCES

[1] R. Menkveld, C. AG. Holleboom, and J. PT. Rhemrev, "Measurement and significance of sperm morphology," *Asian Journal of Andrology*, vol. 13, pp. 59-68, 2011.

[2] D. F. Katz, J. W. Overstreet, S.J Samuels, P. W. Niswander, T. D. Bloom, and E. L. Lewis, "Morphometric analysis of spermatozoa in the assessment of human male fertility", *Journal of Andrology*, vol. 7, pp. 203-210, 1985.

[3] L. Sánchez, N. Petkov, and E. Alegre, "Statistical approach to boar semen evaluation using intracellular intensity distribution of head images", *Cellular and Molecular Biology*, vol. 52, no. 6, pp. 38-43, 2006.

[4] C. G. Gravance, D.L. Garner, C. Pitt, R. Vishwanath, S. K. Sax-Gravance, and P. J. Casey, "Replicate and technician variation associated with computer aided bull sperm head morphometry analysis (ASMA)", *International Journal of Andrology*, vol. 22, pp. 77-82, 1999.

[5] M. Hirai, A. Boersma, A. Hoeflich, E. Wolf, J. Foll, T. Aumuller, and J. Braun, "Objectively measured sperm motility and sperm head morphometry in boars (Sus scrofa): relation to fertility and seminal plasma growth factors," *J. Androl.*, vol. 22, pp. 104-110, 2001.

[6] J. Wijchman, B. D. Wolf, R. Graafe, and E. Arts, "Variation in semen parameters derived from computer-aided semen analysis, within donors and between donors," *J. Androl.,* vol. 22, pp. 773-780, 2001.

[7] A. Quintero-Moreno, T. Rigaub, and J. E. Rodrguez-Gil, "Regression analyses and motile sperm subpopulation structure study as improving tools in boar semen quality analysis", *Theriogenology*, vol. 61, pp. 673-690, 2001.

[8] T. Rijsselaere, A. V. Soom, G. Hoflack, D. Maes, and A. D. Kruif, "Automated sperm morphometry and morphology analysis of canine semen by the Hamilton-Thorne analyser", *Theriogenology*, vol. 62, pp. 1292-1306, 2004.

[9] J. Verstegen, M. Iguer-Ouada, and K. Onclin, "Computer assisted semen analyzers in andrology research and veterinary practice", *Theriogenology*, vol. 57, pp. 149-179, 2001.

[10] M. Beletti, L. Costa, and M. Viana, "A comparison of morphometric characteristics of sperm from fertile bos taurus and bos indicus bulls in Brazil", *Animal Reproduction Science*, vol. 85, pp. 105-116, 2005.

[11] C. Garrett, and H. Baker, "A new fully automated system for the morphometric analysis of human sperm heads", *Fertil. Steril.*, vol. 63, pp. 1306-1317, 1995.

[12] C. Linneberg, P. Salamon, C. Svarer, and L. Hansen, "Towards semen quality assessment using neural networks", In *Proc. IEEE Neural Networks for Signal Processing IV*, pp. 509-517, 1994.

[13] G. Ostermeier, G. Sargeant, T. Yandell, and J. Parrish, "Measurement of bovine sperm nuclear shape using Fourier harmonic amplitudes", *J. Androl.*, vol. 22, pp. 584-594, 2001.

[14] A. Bijar, and M. Mikaeili, "Sperm's tail identification and discrimination in microscopic images of stained human semen smear," In *proceeding of the 7th International Symposium on Image and Signal Processing and Analysis (ISPA), Croatia,*, pp. 709-714, 2011.

[15] L. Sánchez, N. Petkov N, and E. Alegre, "Statistical approach to boar semen head classification based on intracellular intensity distribution," In *A. Gagalowicz, W. Philips (Eds.) Proceedings of the International Conference on Computer Analysis of Images and Patterns, CAIP 2005, Lecture Notes in Computer Science, Springer, Berlin, Heidelberg, 3691,* pp. 88-95.

[16] F. Nowshiravan Rahatabad, M. H. Moradi, and V. R. Nafisi, "A Multi Steps Algorithm for Sperm Segmentation in Microscopic Image," In *proceedings of the World Academy of Science, Engineering and Technology,* pp. 43-45, 2005.

[17] V. R. Nafisi, M. H. Moradi, and M. H. Nasr-Esfahani, "Sperm Identification Using Elliptic Model and Tail Detection," In *proceedings of the World Academy of Science, Engineering and Technology*, pp. 205-208, 2005.

[18] H. Carrillo, J. Villarreal, M. Sotaquira, M. Goelkel, and R. Gutierrez, "A Computer Aided Tool for the Assessment of Humnan Sperm Morphology," In *proceedings of the 7th IEEE International Conference on Bioinformatics and Bioengineering (BIBE)*, pp. 1152-1157, 2007.

[19] H. Carrillo, J. Villarreal, M. Sotaquira, M. Goelkel, and R. Gutierrez, "Spermatozoon Segmentation Towards an Objective Analysis of Human Sperm Morphology," In *proceedings of the 5th International Symposium on image and Signal Processing and Analysis,* pp. 522-527, 2005.

[20] J. Rajan, K. Kannan, and M. R. "Kaimal, An Improved Hybrid Model for Molecular Image Denoising," *Journal of Mathematical Imaging and Vision*, vol. 31, pp. 73-79, 2008.

[21] H. Pirzadeh, "Computational geometry with the rotating calipers," *Master's thesis, School of Computer Science, McGill University, Montreal, Quebec, Canada*, 1999.

[22] G. T. Toussaint, "Solving geometric problems with the rotating calipers", In *Proceedings of IEEE MELECON'83, Athens, Greece*, pp. 1-8, 1999.

[23] A. Andrew, "Another efficient algorithm for convex hulls in two dimensions", Information Processing Letters vol. 9, no. 5, pp. 216-219, 1997.

[24] W. L. Martinez, and A. R. Martinez, "Computational Statistics Handbook with MATLAB," *Chapman and Hall, CRC, London, Boca Raton, FL*, 2002.

[25] R. Khayati, M. Vafadust, F. Towhidkhah, and S. M. Nabavi, "Fully automatic segmentation of multiple sclerosis lesions in brain MR FLAIR images using adaptive mixtures method and markov random field model", *Computers in Biology and Medicine*, vol. 38, pp. 379-390, 2008.

[26] S. Z. Li, "Markov Random Field Modeling in Image Analysis", *Tokyo, Springer,* 2001.

[27] K. Held, E. R. Kops, B. J. Krause, W.M. Wells,and R. Kikinis, H. W. Müller-Gärtner, "Markov random field segmentation of brain MR images", *IEEE Trans. Med. Imag.*, vol. 6, pp. 878-886, 1997.

[28] D. Geman, S. Geman, C. Graffigne, P. Dong, "Boundary detection by constrained optimization. *IEEE Trans. Pattern Anal. Machine Intell.*, vo. 12, no. 7, pp. 609-628, 1990.

[29] C. W. Therrien, "Decision, Estimation, and Classification", *Wiley, New York*, 1989.

[30] J. M. Nett, "The study of MS using MRI, image processing, and visualization," *M.Sc. Thesis, University of Louisville,* 2001.